materials

MDPI

Article

A Statistical Evolution Model of Concrete Damage Induced by Seawater Corrosion

Hangjie Lv [1], Jiankang Chen [1,*] and Chunsheng Lu [2]

[1] Key Laboratory of Impact and Safety Engineering, School of Mechanical Engineering and Mechanics, Ningbo University, Ningbo 315211, China; 1811081010@nbu.edu.cn
[2] School of Civil and Mechanical Engineering, Curtin University, Perth, WA 6845, Australia; C.Lu@curtin.edu.au
* Correspondence: chenjiankang@nbu.edu.cn

Abstract: The transmission of sulfate ions in concrete results in formation of calcium sulfoaluminate crystals due to chemical reactions. The expansion of calcium sulfoaluminate crystals is the main cause of concrete corrosion damage. In this study, ultrasonic analysis was used to detect the modulus change of concrete due to sulfate corrosion to obtain the basic law of corrosion damage evolution. An exponential growth model was developed for the internal expansion force based on the chemical reaction rate of calcium sulfoaluminate crystallization. Then, the evolution equation of the number density of microcracks was derived based on their initiation and balance conditions. Finally, a statistical model was developed for the concrete damage evolution by integrating the volume of microcracks. It is shown that the statistical evolution model can well characterize the evolution of concrete corrosion damage.

Keywords: chemical corrosion; corrosion damage; concrete; statistical evolution; micro-cracks

Citation: Lv, H.; Chen, J.; Lu, C. A Statistical Evolution Model of Concrete Damage Induced by Seawater Corrosion. *Materials* **2021**, *14*, 1007. https://doi.org/10.3390/ma14041007

Academic Editor: Frank Collins

Received: 9 January 2021
Accepted: 11 February 2021
Published: 20 February 2021

1. Introduction

It is well-known that seawater contains a large number of ions that are harmful to concrete, among which sulfate corrosion is one of the most important mechanisms for degradation of concrete's durability in marine environments [1–3]. Expansive stress could be generated due to the chemical reactions between diffused sulfate ions and the pore solution in concrete structures. The stress significantly affects the mechanical properties and durability of cement-based materials [4,5]. The nucleation and growth of microcracks might occur under the action of an internal expansive stress and an external load, which ultimately decreases the service life of concrete structures.

The majority of the previous research on the durability of concrete structures in marine environments has focused on corrosion due to chloride ions [6–8]. Sulfate attack not only induces damage in concrete in marine environments and diminishes its mechanical properties [9], but also supplies more paths for the diffusion of chloride ions. Therefore, sulfate attack on concrete has been one of the most important research subjects in recent decades. Although the harmful effects of sulfate corrosion on concrete structures have been realized for some time, due to the complexity of the problem, relevant research on the corrosion mechanism and damage evolution has been conducted only during the past 20 years; for instance, Adam [10] suggested that sulfate attack on concrete was a "confused word".

Ettringite and gypsum are the major products of sulfate attack that cause expansion of concrete, although the exact mechanism is not fully understood [11–13]. Currently, the most commonly used theories include swelling [14], topological chemical reaction [15], and crystal growth pressure [16,17]. When sulfate ions are diffused in concrete pores, a chemical equilibrium is disturbed between the solid phase and interstitial solution in the cemented matrix [18–20]. Chemical reactions between ions and pore solution produce

gypsum, thaumasite, and delayed ettringite [21–23]. As the corrosion age increases, reaction products gradually accumulate in the pores or interfacial transition zones of concrete, resulting in generation of expansion pressure. In turn, this expansion pressure generates tensile stress. If the stress exceeds the tensile strength of the concrete structure, microcracks nucleate. The evolution of corrosion cracks diminishes the concrete's density and porosity, and this leads to deterioration of the concrete [24]. Because corrosion damage can decrease concrete durability, there have been many studies on this topic. For example, Monteiro and Kurtis [25] studied the time of expansion failure of concrete specimens immersed in sulfate solution. Yang et al. [26] investigated the influence of sulfate attack on variations of the concrete modulus. Wardeh and Toutanji [27] combined elastic and continuum damage mechanics to develop an anisotropic damage model for concrete.

To accurately evaluate the service life of concrete structures under sulfate attack, researchers have proposed several damage models based on variation of the macroscopic mechanical properties of concrete structures. To develop the STADIUM (stands for Software for Transport and Degradation In (Un)saturated Materials) model for sulfate corrosion, Marchand et al. [28] evaluated the effects of various cement types, corrosion solution concentrations, and water–cement ratios on corrosion damage. Sarkar et al. [29] established a mechanical damage model based on the STADIUM model. In this modified model, the process of concrete failure was described in detail and the stress–strain curve of concrete specimens was obtained under sulfate attack. These damage models based on the macroscopic mechanical properties of concrete are valid for the evaluation of concrete damage. Regarding the mesoscopic structure of concrete, however, meso-mechanical models must be based on the meso-physical mechanism of material damage. Thus, the damage effect on the macro properties of materials should be taken into account. The relationship between the macroscopic mechanical behaviors of materials and damage parameters under sulfate attack is of significant importance. Although a macroscopic mechanical property-based concrete damage model is important in damage evaluation, establishing a meso-mechanics model based on the micro-structure of concrete is more reasonable. Researchers have developed several meso-mechanics [30], grid [31], and random aggregate models [32] for evaluation of damage and fracture processes of concrete. As an example, Basista and Weglewski [33] proposed a micromechanical model for deformation simulation of cementitious composites due to external sulfate attack.

In contrast, few reports have been published on the damage evolution of microcracks due to sulfate attack. Microcracks generated by corrosion can be expanded and converged until concrete failure. In addition, macro-damage in materials generated by accumulation of micro-damages may have a catastrophic consequence. In this study, the evolution of corrosion damage of concrete due to sulfate attack was investigated by statistical method, in which the effect of chemical reaction rate was taken into account. Then, a statistical evolution model of corrosion damage of concrete was developed. Results showed the proposed model can well describe the characteristics of corrosion damage evolution.

2. Mathematical Characterization of Corrosion Damage Evolution

The chemical reaction takes place during diffusion of sulfate ions in concrete. The main chemical process includes [34]:

$$CH + SO_4^{2-} \rightarrow C\bar{S}H_2 + 2OH^- \quad (1)$$

and:

$$\begin{aligned} &CA + qCSH_2 \rightarrow C_6A\bar{S}_3H_{32} \\ &CA := \gamma_1C_3A + \gamma_2C_4AH_{13} + \gamma_3C_4A\bar{S}H_{12} \\ &q = 3\gamma_1 + 3\gamma_2 + 2\gamma_3 \end{aligned} \quad (2)$$

where CH and $C\bar{S}H_2$, respectively, denote calcium hydroxide and gypsum; symbols C_4AH_{13} and $C_4A\bar{S}H_{12}$, respectively, represent tetracalcium aluminate and monosulfate; q is the stoichiometric weighted coefficient of the sulfate phase; γ_i (i = 1–3) denotes the proportion of each aluminate phase to the total aluminate content.

The chemical reaction rate equation can be analytically obtained from Equations (1) and (2), that is:

$$\frac{dC_{CA}}{dt} = -\frac{kC_{CA}C_{SO}}{q}\frac{dC_{SO}}{dt} = -kC_{CA}C_{SO} \quad (3)$$

where C_{CA} and C_{SO} are the concentrations of CA and sulfate ions, and k is the coefficient of reaction. Then, we have:

$$\frac{dC_{SO}}{dt} = q\frac{dC_{CA}}{dt} \quad (4)$$

From Equations (3) and (4) we can obtain:

$$\frac{dC_{CA}}{dt} = -kC_{CA}(C_{CA} + \beta_p) \quad (5)$$

Usually, C_{CA} is much less than 1, thus the second order small quantity on the right-hand side of Equation (5) can be neglected; we obtained:

$$\frac{dC_{CA}}{dt} = -k\beta_p C_{CA} \quad (6)$$

As shown in the first formula of Equation (2), the increase in ettringite concentration, $dC_{Ettringite}$, is proportional to the decrease in concentration, dC_{CA}, namely:

$$dC_{Ettringite} \propto -dC_{CA} \quad (7)$$

Generally speaking, the expansive stress appears due to growth of ettringite in pores of concrete. This stress leads to nucleation and growth of microcracks in concrete materials, as observed in Figure 1, where the main crack area is indicated by arrows in the lower-left and upper-right corners. Due to the corrosion effect of sodium sulfate solution, ettringite grew in the crack, with the columnar crystal representing delayed ettringite formation. Due to the expansion effect of ettringite, the main crack area continuously expanded and another crack was generated along the internal expansion direction. This suggests that concrete damage may be caused by expansion stress produced by delayed ettringite.

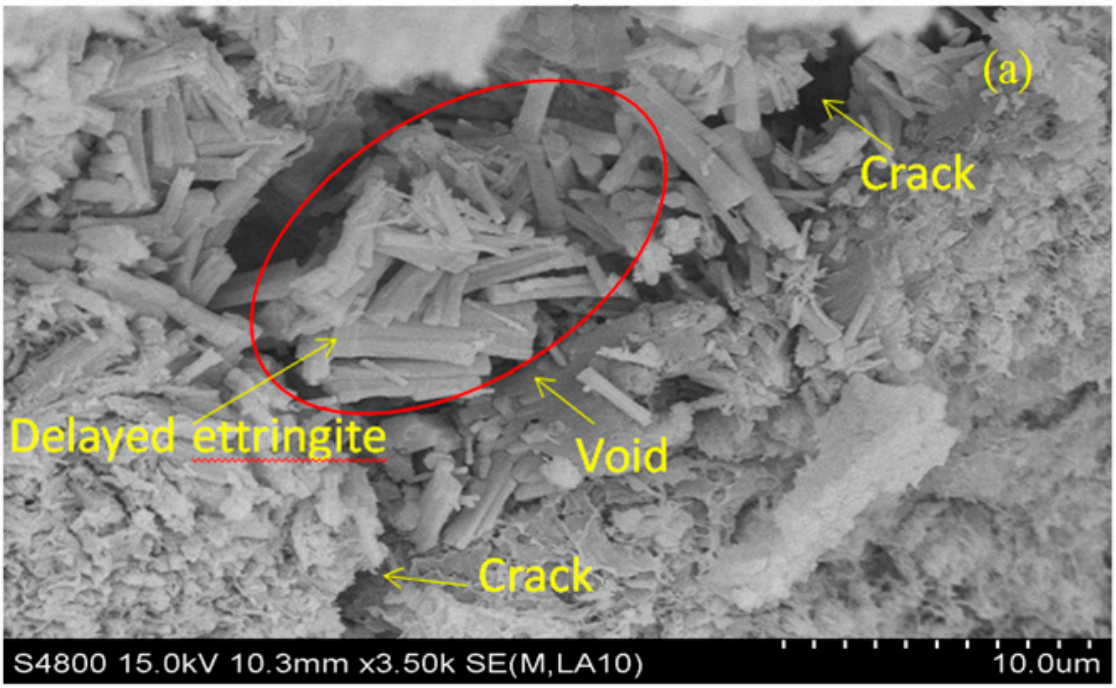

Figure 1. *Cont.*

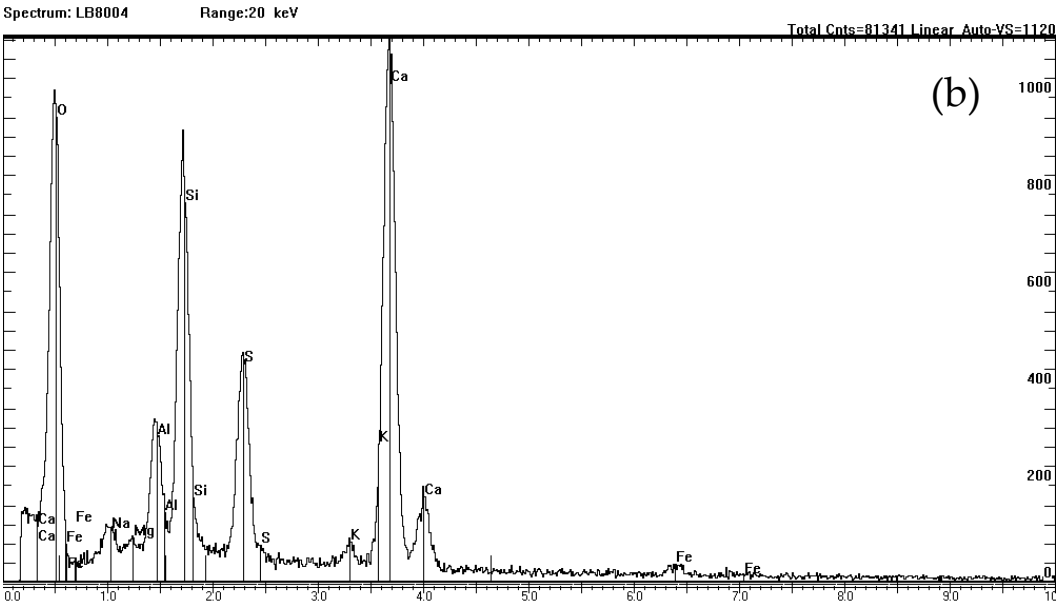

Figure 1. (**a**) SEM image of damage in a concrete sample immersed in sodium sulfate solution with 8% concentration for 250 days, and (**b**) the energy spectrum of ettingite.

Here let us assume that the number density of microcracks in concrete at time t of service is [35,36]:

$$n = n(t,\ a) \tag{8}$$

The definition given by Equation (1) means the number of cracks with length $[a, a + \mathrm{d}a]$ perunit volume is $n(t, a)\mathrm{d}a$.

Chen et al. [37] proposed an empirical formula to describe the corrosion damage evolution. The damage degree D is defined as the volume occupied by microcracks per unit volume. Therefore, D can be considered as the sum of all crack volumes in a unit volume of concrete, that is:

$$\mathrm{D} = \int_0^\infty n(t,\ a)\beta_a a^3 \mathrm{d}a \tag{9}$$

where β_a is a dimensionless parameter.

Concrete degradation due to corrosion mainly includes the nucleation, growth, and convergence of microcracks (see Figure 2). However, macrocracks are formed at the crack convergence stage, indicating that the concrete structure has to be repaired. Therefore, this study is mainly focused on the statistical evolution of the nucleation and growth of microcracks.

Figure 2. Corrosion cracks on surface of a concrete sample immersed in sodium sulfate solution of 8% concentration for 250 days.

Bai et al. [35] found that the nucleation rate of microcracks, $\dot{n}_N$, is related to the local stress σ_t and the crack length a, which can be well described as:

$$\dot{n}_N = k_{th}\left(\frac{\sigma_t}{\sigma_{th}} - 1\right)\left(\frac{a}{a_{th}}\right)\exp\left[-\left(\frac{a}{a_{th}}\right)^m\right], \ (\sigma_t > \sigma_{th}) \tag{10}$$

where k_{th} and m are material constants, a_{th} is the reference length,σ_{th} is the threshold stress of microcrack nucleation, and σ_t is a function of the external load and corrosion factor.

Corrosion can be converted into an internal expansion force p through chemical mechanics. Therefore, σ_t can be expressed as the superposition of an external load and an internal expansion force, that is:

$$\sigma_t = \sigma_0 + \beta_p p \tag{11}$$

where β_p is a proportional coefficient describing the effect of corrosion factor, and σ_0 is stress caused by the external load. The latter can be determined by the second invariant of far-field stress deflection $J'_{2(\mathrm{Rem})}$, and we have:

$$\sigma_0 = \beta_\sigma \sqrt{3J'_{2(\mathrm{Rem})}} \tag{12}$$

where β_σ is a proportional coefficient.

The internal expansion force, the second term on the right-hand side of Equation (10), is derived by using the chemical reaction rate of delayed ettringite formation. Here, it is assumed that the increase in expansion stress dp is proportional to the increase in delayed ettringite concentration,d$C_{\mathrm{Ettringite}}$, namely:

$$\mathrm{d}p \propto \mathrm{d}C_{\mathrm{Ettringite}} \tag{13}$$

Then, according to Equations (7) and (13), we can obtain:

$$C_{\mathrm{CA}} = -\lambda(p - p*) \tag{14}$$

where λ and $p*$ are the parameters to be determined.

Substituting Equation (14) into Equation (6), we have:

$$\frac{\mathrm{d}(p - p*)}{\mathrm{d}t} = -k\beta_p(p - p*) \tag{15}$$

Solving Equation (15) for p, we obtain:

$$p = p^*[1 - \exp(-t/t_p)] \tag{16}$$

where t_p is the characteristic time.

Based on the results obtained by Seaman et al. [38] and Stenvens et al. [39], the microcrack growth equation is derived as:

$$\begin{aligned} \dot{a} &= g(t)a \\ g(t) &= (\sigma_t - \sigma_{th})/4\eta \end{aligned} \tag{17}$$

where η is the viscosity coefficient.

Based on the number balance principle of microcracks between [a, a+da], a partial differential equation is obtained [35], that is:

$$\frac{\partial n}{\partial t} + \frac{\partial(\dot{a}n)}{\partial a} = \dot{n}_N \tag{18}$$

Substituting Equation (17) into Equation (18) yields:

$$\frac{\partial n}{\partial t} + \frac{\partial n}{\partial a}\dot{a} + g(t) = \dot{n}_N \tag{19}$$

Such a first-order partial differential equation can be transformed into a first-order ordinary differential equation on the characteristic line. Then, the evolution equation of the number density of microcracks can be written as:

$$\frac{\mathrm{d}n}{\mathrm{d}t} + g(t)n = \dot{n}_N \tag{20}$$

Multiplying both sides of Equation (20) by $\beta_a a^3$ and integrating it gives:

$$\int_0^\infty \beta_a a^3 \frac{\mathrm{d}n}{\mathrm{d}t}\mathrm{d}a + \int_0^\infty g(t) n \beta_a a^3 \mathrm{d}a = \int_0^\infty \dot{n_N} \beta_a a^3 \mathrm{d}a \tag{21}$$

From Equation (9), it is seen that Equation (21) can be rewritten as:

$$\frac{\mathrm{d}D}{\mathrm{d}t} + g(t)D = Q(t,a) \tag{22}$$

$$Q(t,a) = \int_0^\infty \dot{n}_N \beta_a a^3 \mathrm{d}a \tag{23}$$

Solving Equation (22) and noting $D|_{t=0}$, the damage evolution under sulfate attack and external loading can be obtained as:

$$D = e^{-\int g(t)\mathrm{d}t} \int_0^t Q(\tau,a)\, e^{\int g(t)\mathrm{d}t} \mathrm{d}\tau \tag{24}$$

If the effect of remote loads is not taken into account, the parameter β_σ in Equation (12) should be zero.

3. Experimental

To detect the evolution of corrosion damage expressed by Equation (24), concrete can be approximately regarded as a composite composed of a concrete matrix and corrosion cracks. As illustrated in Figure 3, there is an expansive force in corrosion cracks.

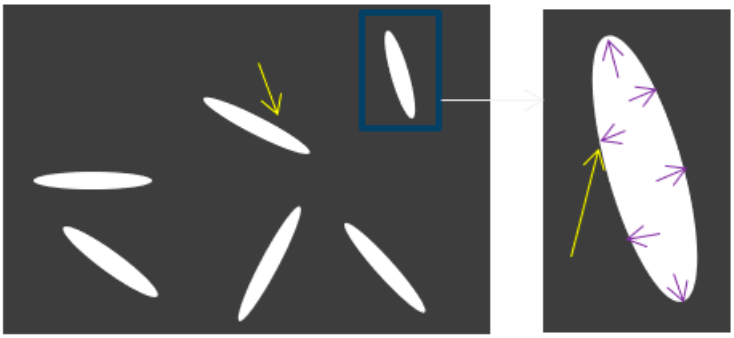

Figure 3. Schematic representation of concrete after corrosion, where the loading condition is shown in a partially enlarged crack (right).

The concrete modulus after corrosion, E, is determined by means of the volume average, that is:

$$E = \frac{1}{V}\int_V E_0 \mathrm{d}V = \frac{V - V_C}{V} E_0 = \left(1 - \frac{V_C}{V}\right) E_0 \tag{25}$$

where V and V_C are the volume of concrete and the total volume of corrosion cracks, and E_0 is the modulus of concrete matrix (or concrete before corrosion).

Note that V_C/V is the volume occupied by cracks per unit volume, which is equal to the corrosion damage, D. Hence, Equation (25) can be written as:

$$D = 1 - \frac{E}{E_0} \tag{26}$$

3.1. Experimental Materials and Sample Preparation

Po42.5 cement, produced by Yangzhou Lvyang Cement Co. Ltd., Yangzhou, China, was applied for the preparation of test specimens. The sodium sulfate solution for corrosion was prepared manually. Analytical grade pure sodium sulfate (from Shanghai Chemical Reagent Company of China Pharmaceutical (Group)) was used with a molecular weight of 142.04.

The water-to-cement ratio has a significant influence on the mechanical properties of cement mortar. Therefore, mortar specimens with different water-to-cement ratios were prepared to determine their relationships with the mechanical properties of mortar. As listed in Table 1, standard specimens with dimensions of 150 × 150 × 150 mm^3 were used to determine the dynamic elastic modulus, and specimens with dimensions 10 × 10 × 70 mm^3 were used for SEM tests to observe microstructures of concrete specimens.

Table 1. Mix proportions of mortar, where H and Z indicate specimens for dynamic tests and microstructural observation, respectively.

Sample	Cement	Sand	*w/c*
H1	1	3	0.4
H3	1	3	0.7
Z	1	2	0.45

3.2. Experimental Scheme

Cement mortar specimens were kept under the environmental conditions of 20 °C and 90% humidity for 24 h and, then, were transferred to a standard curing room for 28 d after removing formworks. These specimens were evenly divided into three groups and soaked sodium sulfate [SO_4^{2-}] solutions with three different concentrations of 0%, 3%, and 8%, to detect the dynamic elastic moduli of specimens on 14 d, 28 d, 60 d, 90 d, . . . , and 450 d, respectively.

3.3. Testing Method of Dynamic Elastic Modulus

The test method of the dynamic elastic modulus consists of several steps. First, a relatively complete surface of a sample was taken as a benchmark. Then, ultrasonic wave velocities at five points were measured at four points near the vertex and one point in the middle, as illustrated in Figure 4, in which, the symbol "*v*" denotes the ultrasonic wave speed. Finally, the average value of five points was reported.

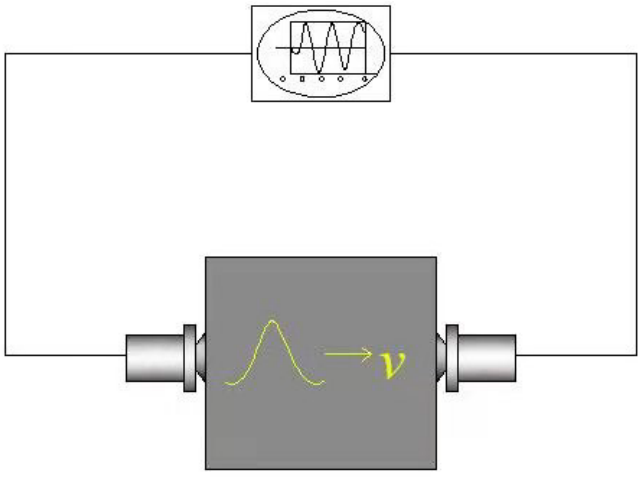

Figure 4. Illustration of an ultrasonic testing method of dynamic elastic modulus.

4. Results and Discussion

4.1. Experimental Results

The dynamic elastic modulus was measured at several intervals. The obtained results are shown in Figures 5 and 6.

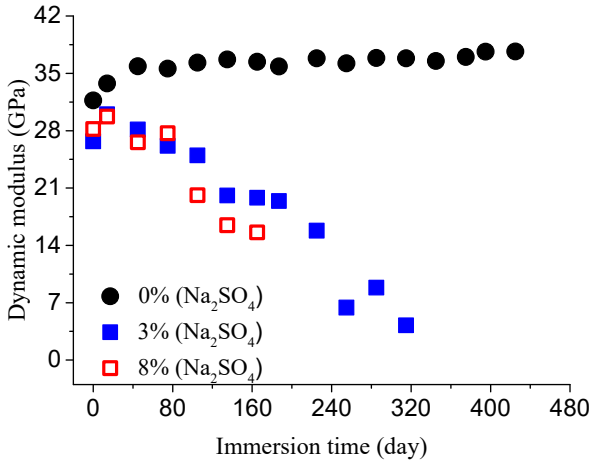

Figure 5. Dynamic modulus evolution of concrete specimens with the water-to-cement ratio of 0.4 in different concentrations of sodium sulfate solution.

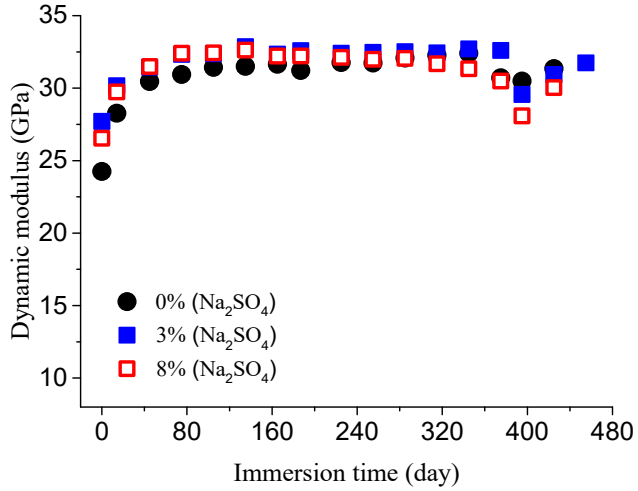

Figure 6. Dynamic modulus evolution of concrete specimens with the water-to-cement ratio of 0.7 in different concentrations of sodium sulfate.

As you can see from Figures 5 and 6, the increase in the modulus is due to continuous hydration of concrete and the filling effect of delayed ettringite, which results in negligible concrete damage. With the increase in corrosion time, the modulus begins to decrease. This is due to the corrosion damage evolution.

4.2. Experimental Determination of Corrosion Damage Model Parameters

By neglecting the effect of continuous hydration, the evolution of the concrete dynamic modulus can be determined, as shown in Figures 7 and 8.

Based on these experimental results, the concrete damage evolution under sulfate attack can be obtained by Equation (26), as plotted in Figure 9.

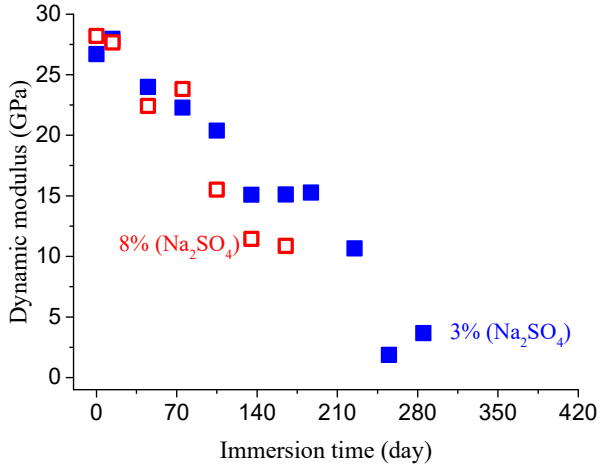

Figure 7. Dynamic modulus evolution of concrete specimens (w/c = 0.4) after eliminating hydration in different sulfate solutions.

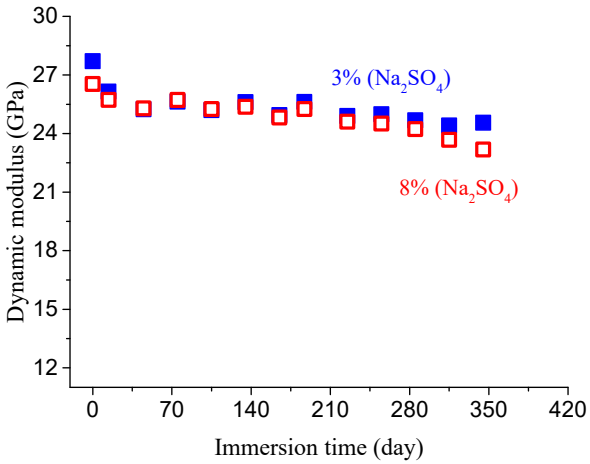

Figure 8. Dynamic modulus evolution of concrete specimens (w/c = 0.7) after eliminating hydration in different sulfate solution.

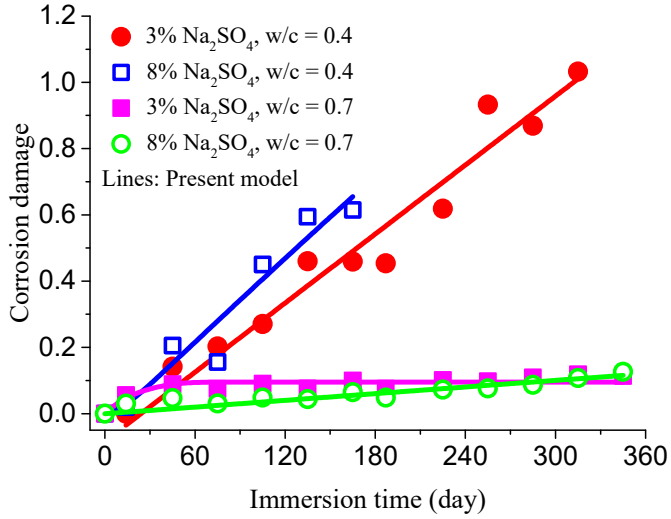

Figure 9. Damage evolution results of concrete specimens.

From Equation (10) and Equation (23), we have:

$$\begin{aligned} Q(t,a) &= \int_0^\infty \dot{n}_N \beta_a a^3 \mathrm{d}a = \int_0^\infty k_{th}\beta_a \left(\frac{\sigma_t}{\sigma_{th}} - 1\right)\left(\frac{a}{a_{th}}\right) \exp\left[-\left(\frac{a}{a_{th}}\right)\right] a^3 \, \mathrm{d}a \\ &= 24 k_{th}\beta_a \left(\frac{\sigma_0 + P_0^*\left[1-\exp(-t/t_p)\right]}{\sigma_{th}} - 1\right) \end{aligned} \tag{27}$$

Substituting Equation (11) into Equation (17) gives:

$$g(t) = \frac{\sigma_0 + P_0^*\left[1 - \exp\left(-t/t_p\right)\right] - \sigma_{th}}{4\eta} \tag{28}$$

Therefore, we can obtain:

$$\int g(t) \, \mathrm{d}t = \frac{\sigma_0 - \sigma_{th}}{4\eta} t + \frac{P_0^*}{4\eta} t + \frac{\exp(-t/t_p) P_0^* t_p}{4\eta} \tag{29}$$

By substitution of Equations (29) and (27) into Equation (24), the expression of damage evolution can be derived under the simultaneous action of external load and corrosion factors. Considering the damage evolution of concrete only under sulfate, i.e., $\sigma_0 = 0$, we have:

$$\begin{aligned} &D = \tfrac{96\eta k}{\sigma_{th}}[\varsigma + \exp(\psi(t))] \cdot \exp(-\psi(t)) \\ &k = k_{th}\beta_a, \ \varsigma = -\exp\left(P_0^* t_p / 4\eta\right) \\ &\psi(t) = \left(P_0^* t_p \cdot \exp\left(-t/t_p\right) + \left(P_0^* - \sigma_{th}\right) t\right)/4\eta \end{aligned} \tag{30}$$

Here, the threshold stress σ_{th}= 4 MPa of microcrack nucleation was determined with the design value of axial tensile strength of concrete. Using Equation (30), the specific fitting results are shown in Figure 9.

It is seen that experimental results are consistent with those obtained from the damage model. When concrete specimens are exposed to sulfate attack, the internal damage evolution law of concrete is also in agreement with the model given by Equation (30). Therefore, such a modified model can be applied to characterize the internal damage evolution law of concrete.

5. Conclusions

It was theoretically proven that the increase in the space occupied by corrosion cracks per unit volume is equivalent to the reduction of the concrete modulus due to corrosion. Therefore, it is reasonable to use ultrasonic technology to detect changes in concrete modulus to analyze damage evolution.

(1) By combining the equilibrium equation of microcrack number density evolution and the chemical reaction rate equation, the first-order partial differential equations were derived. The corrosion damage evolution model of concrete under sulfate attack was developed by integrating the volume of microcrack number density.
(2) The new corrosion damage model established in this paper is able to accurately describe the internal damage evolution process of concrete under sulfate corrosion. The analysis method proposed in this paper provides a reference for the corrosion damage analysis of other materials.

Author Contributions: Conceptualization, J.C.; methodology, J.C. and C.L.; software, H.L.; validation, C.L., J.C. and H.L.; formal analysis, J.C.; investigation, H.L.; resources, J.C.; data curation, H.L.; writing—original draft preparation, H.L. and J.C.; writing—review and editing, J.C. and C.L.; visualization, H.L., J.C. and C.L.; supervision, J.C.; project administration, J.C.; funding acquisition, J.C. All authors have read and agreed to the published version of the manuscript.

Funding: This work has been supported by the National Natural Science Foundation of China (NSFC#11772164 and #11832013), the National Basic Research Program of China (973 Program, 2009CB623203), the Marine Biotechnology and Marine Engineering Discipline Group in Ningbo University, and K.C. Wong Magna Fund in Ningbo University.

Conflicts of Interest: The authors declare no conflict of interest.

References

1. Campos, A.; López, C.M.; Aguado, A. Diffusion-reaction model for the internal sulfate attack in concrete. *Constr. Build. Mater.* **2016**, *102*, 531–540. [CrossRef]
2. Zhao, G.W.; Li, J.P.; Shi, M.; Fan, H.H.; Cui, J.F.; Xie, F. Degradation mechanisms of cast-in-situ concrete subjected to internal-external combined sulfate attack. *Constr. Build. Mater.* **2020**, *248*, 118683.
3. Choudhary, A.; Malik, M.; Tiwari, S.; Dubey, A.; Sharma, U.; Kumar, A. Concrete Deterioration Due to Sulphate—A Case Study. In Proceedings of the 8th International Conference on Materials Processing and Characterization (ICMPC 2018), Hyderabad, India, 16–18 March 2018; Elservier: Amsterdam, The Netherlands, 2018; Volume 5, pp. 17952–17957.
4. Ouyang, W.Y.; Chen, J.K.; Jiang, M.Q. Evolution of surface hardness of concrete under sulfate attack. *Constr. Build. Mater.* **2014**, *53*, 419–424.
5. Liu, T.; Zou, D.; Teng, J.; Yan, G. The influence of sulfate attack on the dynamic properties of concrete column. *Constr. Build. Mater.* **2012**, *28*, 201–207.
6. Angst, U.M. Predicting the time to corrosion initiation in reinforced concrete structures exposed to chlorides. *Cem. Concr. Res.* **2019**, *115*, 559–567.
7. Wu, Z.Y.; Yu, H.F.; Ma, H.Y.; Zhang, J.H.; Da, B.; Zhu, H.W. Rebar corrosion in coral aggregate concrete: Determination of chloride threshold by LPR. *Cem. Concr. Res.* **2020**, *163*, 108238.
8. Jiang, B.Z.; Doi, K.; Tsuchiya, K.; Kawano, Y.; Kori, A.; Ikushima, K. Micromechanical properties of steel corrosion products in concrete studied by nano-indentation technique. *Corros. Sci.* **2020**, *163*, 108304.
9. Pinto, S.R.; Da Luz, C.A.; Munhoz, G.S.; Medeiros, R.A., Jr. Durability of phosphogypsum-based supersulfated cement mortar against external attack by sodium and magnesium sulfate. *Cem. Concr. Res.* **2020**, *136*, 106172.
10. Neville, A. The confused world of sulfate attack on concrete. *Cem. Concr. Res.* **2004**, *34*, 1275–1296.
11. Cohen, M.D. Theories of expansion in sulfoaluminate-type expansive cements: Schools of thought. *Cem. Concr. Res.* **1983**, *13*, 809–818.
12. Brown, P.W.; Taylor, H.F.W. The Role of Ettringite in External Sulfate Attack. In *Material Science of Concrete: Sulfate Attack Mechanisms*; Skalny, J., Marchand, J., Eds.; American Ceramic Society: Westerville, OH, USA, 1999; pp. 73–98.
13. Hansen, W.C. Crystal growth as a source of expansion in Portland cement concrete. *Proc. ASTM* **1963**, *63*, 932–945.
14. Mehta, P.K. Mechanism of expansion associated with ettringite formation. *Cem. Concr. Res.* **1973**, *3*, 1–6.
15. Lafuma, H. Theory of the expansion of hydraulic binders. *Rev. Mater. Constr. Trav. Public* **1929**, *243*, 441–444.
16. Scherer, G.W. Crystallization in pores. *Cem. Concr. Res.* **1999**, *29*, 1347–1358.
17. Scherer, G.W. Stress from crystallization of salt. *Cem. Concr. Res.* **2004**, *34*, 1613–1624.
18. Glasser, F.P. The Thermodynamics of Attack on Portland Cement with Special Reference to Sulfate. In Proceedings of the International RILEM TC-211-PAE Final Conference, Toulouse, France, 3–5 June 2009; Springer: Berlin/Heidelberg, Germany, 2009; Volume 1, pp. 3–17.
19. Fernandes, I.; Broekmans, M.A.T.M. Alkali–Silica Reactions: An Overview. *Metallogr. Microstruct. Anal.* **2013**, *24*, 257–267.
20. Thorvaldson, T. Chemical Aspects of the Durability of Cement Products. Proceedings of 3rd International Symposium on the Chemistry of Cement and Concrete Association, London, UK, 15–20 September 1952; pp. 436–465.
21. Hekal, E.E.; Kishar, E.; Mostafa, H. Magnesium sulfate attack on hardened blended cement pastes under different circumstances. *Cem. Concr. Res.* **2002**, *32*, 1421–1427.
22. Massazza, F. Pozzolanic cements. *Cem. Concr. Compos.* **1993**, *15*, 185–214.
23. Kurdowski, W. Durability of Blended Cements in Aggressive Media. In *Mineral Admixtures in Cement and Concrete*; Sarkar, S.L., Ed.; CRC Press: Boca Raton, FL, USA, 1993; Volume 4, pp. 448–466.
24. Sahmaran, M.; Erdem, T.K.; Yaman, I.O. Sulfate resistance of plain and blended cements exposed to wetting–drying and heating–cooling environments. *Constr. Build. Mater.* **2007**, *21*, 1771–1778.
25. Monteiro, P.J.M.; Kurtis, K.E. Time to failure for concrete exposed to severe sulfate attack. *Cem. Concr. Res.* **2003**, *33*, 987–993.
26. Yang, D.Y.; Luo, J.J. The damage of concrete under flexural loading and salt solution. *Constr. Build. Mater.* **2012**, *36*, 129–134.
27. Wardeh, M.A.; Toutanji, H.A. Parameter estimation of an anisotropic damage model for concrete using genetic algorithms. *Int. J. Damage Mech.* **2015**, *6*, 801–825.
28. Marchand, J.; Samson, E.; Maltais, Y.; Beaudoin, J.J. Theoretical analysis of the effect of weak sodium sulfate solutions on the durability of concrete. *Cem. Concr. Compos.* **2002**, *24*, 317–329.
29. Sarkar, S.; Mahadevan, S.; Meeussen, J.; van der Sloot, H.; Kosson, D. Numerical simulation of cementitious materials degradation under external sulfate attack. *Cem. Concr. Compos.* **2010**, *32*, 241–252.
30. Mohamed, A.R.; Hansen, W. Micromechanical modeling of crack-aggregate interaction in concrete materials. *Cem. Concr. Compos.* **1999**, *21*, 349–359.
31. Chiaia, B.; Vervuurt, A.; van Mier, J. Lattice model evaluation of progressive failure in disordered particle composites. *Eng. Fract. Mech.* **1997**, *57*, 301–318.
32. Liu, G.; Wang, Z. Simulation of the fracture of concrete with random aggregate model. *J. Tsinghua Univ.* **1996**, *1*, 84–89.
33. Basista, M.; Weglewski, W. Chemically Assisted Damage of Concrete: A Model of Expansion Under External Sulfate Attack. *Int. J. Damage Mech.* **2009**, *18*, 155–175.

34. Ikumi, T.; Cavalaro, S.H.P.; Segura, I.; Aguado, A. Alternative methodology to consider damage and expansions in external sulfate attack modeling. *Cem. Concr. Res.* **2014**, *63*, 105–116.
35. Bai, Y.; Xia, M.; Ke, F. *Statistical Meso-Mechanics of Damage and Failure: How Microdamage Induces Disaster*; Science Press: Beijing, China; Springer Nature: Singapore, 2019; pp. 265–290.
36. Lu, C.; Vere-Jones, D.; Takayasu, H. Avalanche behaviour and statistical properties in a microcrack coalescence process. *Phys. Rev. Lett.* **1999**, *82*, 347–350.
37. Chen, J.K.; Jiang, M.Q.; Zhu, J. Damage evolution in cement mortar due to erosion of sulphate. *Corros. Sci.* **2008**, *50*, 2478–2483.
38. Seaman, L.; Curran, D.R.; Shockey, D.A. Computational models for ductile and brittle fracture. *J. Appl. Phys.* **1976**, *47*, 4814–4826.
39. Stenvens, A.L.; Davison, L.; Warren, W.G. *Dynamic Crack Propagation*; Sih, G.C., Ed.; Noordnoff Uitgevers: Groningen, The Netherlands, 1973.